



## Electrolysis of Molten Iron Oxide with an Iridium Anode: The Role of Electrolyte Basicity

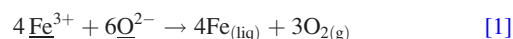
Hojong Kim,<sup>\*</sup> James Paramore,<sup>\*</sup> Antoine Allanore,<sup>\*</sup> and Donald R. Sadoway,<sup>\*,z</sup>

Department of Materials Science and Engineering, Massachusetts Institute of Technology, Cambridge, Massachusetts 02139-4307, USA

Molten oxide electrolysis (MOE) is a carbon-free, electrochemical technique to decompose a metal oxide directly into liquid metal and oxygen gas. From an environmental perspective what makes MOE attractive is its ability to extract metal without generating greenhouse gases. Hence, an inert anode capable of sustained oxygen evolution is a critical enabling component for the technology. To this end, iridium has been evaluated in ironmaking cells operated with two different electrolytes. The basicity of the electrolyte has been found to have a dramatic effect on the stability of the iridium anode. The rate of iridium loss in an acidic melt with high silica content has been measured to be much less than that in a basic melt with high calcia content.  
© 2011 The Electrochemical Society. [DOI: 10.1149/1.3623446] All rights reserved.

Manuscript submitted May 31, 2011; revised manuscript received July 15, 2011. Published August 5, 2011.

Electrolysis is being investigated by the steel industry as a carbon-lean route that copes with the potential environmental constraints on emissions.<sup>1-3</sup> Of all the new methods under consideration, only molten oxide electrolysis (MOE) produces liquid metal,<sup>4,5</sup> which occurs by the decomposition of iron oxide dissolved in an appropriately designed solvent melt according to



The reduction mechanism of MOE is similar to that of the Hall-Héroult process for aluminum production, which consists of the electrolytic decomposition of aluminum oxide dissolved in a molten fluoride solvent comprising cryolite. However, the two processes are fundamentally different with regards to the compensating oxidation reaction at the anode. In the Hall-Héroult cell, oxidation requires the attendant consumption of the carbon anode resulting in the generation of carbon dioxide. In MOE the compensating reaction is the generation of oxygen, which is predicated on the existence of a so-called inert anode whose development is nontrivial given the extreme conditions in the cell including:

- temperatures in excess of the melting point of iron (1538°C)
- high solubilizing power of a multicomponent oxide melt
- evolution of pure oxygen gas at atmospheric pressure.

Furthermore, to meet the production requirements of an industrial process, the anode must sustain high current densities, potentially exceeding 1 A cm<sup>-2</sup>. Under these conditions, most metals are poor candidates due to the oxidizing atmosphere surrounding the anode and the extreme anodic potential to which the electrode is subjected. Furthermore, passivating oxide layers, which would normally protect a metallic surface, are dissolved by the molten oxide electrolyte resulting in unabated oxidation of the metal.<sup>6,7</sup>

Previous work in this laboratory demonstrated that iridium can serve as an oxygen-evolving anode.<sup>4,8</sup> Furthermore, the anodic current density and, hence, the rate of oxygen evolution was found to increase with the optical basicity of the electrolyte at a given value of potential. The focus of the present study is the assessment of the chemical stability of iridium as a function of electrolyte composition. While the cost and scarcity of this metal make it unsuitable for industrial applications, it has a role to play in laboratory-scale studies of new metallurgical processes.

The electrolytes investigated in the present study are composed of five oxides. The solvent or so-called supporting electrolyte contains silica, alumina, magnesia, and calcia. Iron oxide (Fe<sub>2</sub>O<sub>3</sub>) is added to the melt at a concentration of 9.1 wt % as feedstock for ironmaking. It is convenient to express the melt chemistry of this quinary system in terms of its Lewis acid-base properties according

to a scale of optical basicity. In an oxide melt, silica polymerizes and acts as an electron-pair acceptor; hence, melts high in silica are termed acidic and have low values of optical basicity. Dissociating into alkaline-earth cations and oxide anions, magnesia and calcia act as electron-pair donors; thus, melts high in magnesia or calcia are termed basic and have high values of optical basicity. Electrolyte composition is optimized to meet a plurality of constraints. For example, the melting point of the slag<sup>1</sup> must be less than 1450°C. This can be achieved with an acidic slag or a basic slag. However, the values of electrical conductivity and viscosity can be very different, even though the liquidus temperature is nearly identical. To conclusively investigate the utility of iridium as an inert anode material for MOE, a systematic investigation of its stability has been conducted as a function of the electrolyte composition during galvanostatic electrolysis at high anodic current density.

### Experimental

**Electrolytes or slags.**—To perform the electrolysis of iron oxide (Fe<sub>2</sub>O<sub>3</sub>) in an oxide melt, it must be an ionic conductor, be free of elements nobler than iron, have a low vapor pressure, have a suitable melting temperature, and be less dense than liquid iron.<sup>9,10</sup> Based on these criteria, electrolytes containing oxides of SiO<sub>2</sub>-CaO-MgO-Al<sub>2</sub>O<sub>3</sub> were selected for the electrolysis of iron oxide. Two compositions were selected as supporting electrolytes, an acidic slag (Slag A) and a basic slag (Slag B). The compositions and selected properties of these slags are compiled in Table I. High purity oxide powders (99.7 wt % purity min., from Alfa Aesar and Sigma Aldrich) were mixed by manual shaking for approximately 10 min before loading into crucibles. No pre-melting steps were conducted. Physicochemical properties have been evaluated from the reference textbook SLAG ATLAS,<sup>11</sup> mostly by interpolating existing data. However, the validity of this method is not confirmed, and these values must be viewed as approximations. The basicity of slag was determined using the optical basicity scale in the literature.<sup>12,13</sup> Melting points have been determined by FactSage.<sup>14</sup>

**Crucibles.**—High purity alumina (99.8 wt %, McDanel Advanced Ceramics, USA) and magnesia (99.8 wt %, Ozark Technical Ceramics, USA) straight-wall crucibles (6.35 cm diameter, 14 cm height) were used as containers for acidic and basic melts, respectively. An outer molybdenum crucible served as a protection vessel to prevent damage to the furnace in case of ceramic crucible failure.

**Electrodes.**—The anode consisted of a plate of high-purity iridium (>99.9%, Furuya Metals, Japan) 3 × 2.25 × 0.1 cm (total surface area of 6.8 cm<sup>2</sup>). This plate was welded to a molybdenum rod (0.48 cm diameter, 91.4 cm height, American Elements, USA) that served as a current lead. The cathode was a molybdenum disk (3.81

<sup>\*</sup> Electrochemical Society Active Member.

<sup>z</sup> E-mail: dsadoway@mit.edu

<sup>1</sup> In this paper the term “slag” is used interchangeably with “electrolyte.”

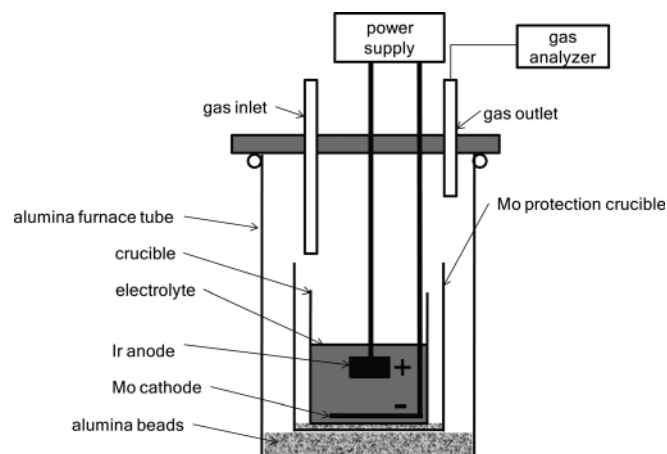
**Table I. Composition (mol %) and properties of selected oxide melts at 1500°C for iron decomposition.**

	SiO <sub>2</sub>	CaO	MgO	Al <sub>2</sub> O <sub>3</sub>	T <sub>m</sub> (°C)	Viscosity (Pa.s)	Density (g cm <sup>-3</sup> )	Conductivity (S cm <sup>-1</sup> )	Melt basicity
Slag A (high silica slag)	45.6	19.1	23.6	11.7	1311	~1	~2.7	~0.2	0.606
Slag B (high calcia slag)	—	57.9	10.3	31.8	1400	~0.27	~2.7	~0.6	0.753

cm diameter, 0.1 cm thickness, surface area facing the anode of 11.4 cm<sup>2</sup>, connected to a threaded molybdenum rod (same dimensions as the anode lead) by a molybdenum nut. All molybdenum rods were protected by high-purity alumina tubes, and connections were protected by high-purity alumina paste (Resbond 989, Cotronics Corp., USA). The electrode was not subjected to any mechanical or chemical pretreatment. As the anode was held vertically above the horizontal cathode disk, the anode surface facing the cathode was limited to 0.3 cm<sup>2</sup>.

**Process operation.**—The crucible and electrodes were sealed from the atmosphere and placed in a closed-one-end alumina tube (11.4 cm inner diameter, 1 m height, 99.8%, McDanel Advanced Ceramics, USA). Temperature was controlled by a furnace equipped with lanthanum chromite heating elements (Model: PVT 18/100/350, Carbolite, UK). The schematic of the experimental set-up is shown in Fig. 1. The furnace temperature controller was set at 1600°C, with a ramping rate of 84°C h<sup>-1</sup>. The type-B thermocouple connected to the temperature controller was located at the outside surface of the alumina tube. The process temperature was measured to be 1550°C in the crucible zone. The concentration of oxygen in the gas atmosphere of the tube was less than 10 ppm due to a continuous flow of high purity argon (99.9999%, Airgas) at approximately 150 cm<sup>3</sup> min<sup>-1</sup>. The oxygen concentration at the gas outlet of the furnace was analyzed by an electrochemical sensor (Rapidox 3100, Cambridge Sensotec, UK).

After 1 hour of equilibration at the target temperature of 1600°C, the molybdenum cathode was first lowered to the bottom of the crucible. The iridium anode was then lowered until it touched the cathode, as confirmed by electrical short-circuit, and then raised by 2 cm to create the desired anode/cathode separation. Galvanostatic electrolysis was conducted at 3.5 A (ParStat 2273, Princeton Applied Research) for 4 h, the corresponding coulombic charge passed being 50,400 C. The current density was 0.3 A cm<sup>-2</sup> on the cathode and 11.7 A cm<sup>-2</sup> on the anode assuming that only the geometric surface facing each electrode was active. After 4 h of electrolysis, the anode and cathode were raised above the electrolyte to prevent back reaction during cooling and to minimize entrainment of electrolyte which would hinder post-mortem analysis of electrodes.

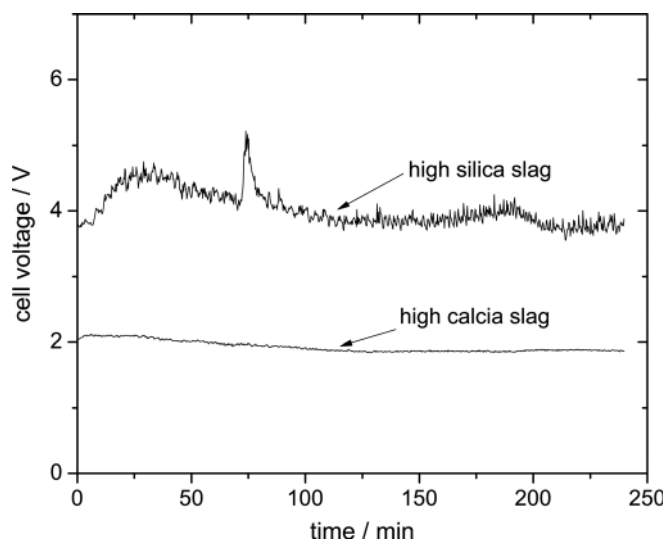
**Figure 1.** Schematic of experimental set-up (not to scale).

**Post-mortem Analysis.**—After the experiment, the system was disassembled for detailed characterization by scanning electron microscopy (SEM, LEO VP 438) and energy dispersive spectroscopy (EDS). The iridium anode was separated from its electrical lead and weighed to determine weight loss. Cross-sections of both electrodes and bulk electrolyte near the center of the crucible were obtained by cutting with a diamond saw, mounting in thermosetting phenolic resin, and polishing using SiC paper and alumina powder down to 0.3 μm.

## Results

**Constant current electrolysis.**—The variation of voltage with time under galvanostatic electrolysis (3.5 A) is presented in Fig. 2. These results are representative of several runs in each electrolyte. The average cell voltage in high-silica electrolyte is twice that measured for high-calcia electrolyte, which is in agreement with expectation based on differences in electrical conductivity data from the literature.<sup>11</sup> A steady-state regime is rapidly observed in the high-calcia electrolyte, contrary to what is observed in the silicate-based system. In the high-calcia melt the voltage is fairly constant, and no fast oscillations can be detected. In the high-silica melt, after an initial increase over 30 min, the cell voltage slowly decreases. Several spikes are seen, as well as a small, high-frequency oscillation in the cell voltage. Altogether, these observations are consistent with the effect of high electrolyte viscosity. Additionally, the spikes may be related to the formation of large gas bubbles in the electrolyte, the removal of which is hindered by the high viscosity, causing a large increase in the local electrical resistivity.

The oxygen content of the outlet gas has been quantified during a separate electrolysis experiment in high-silica melt, as reported in Fig. 3. The classical bell-shape of the signal is related to the gradual filling of the analyzing system with oxygen, the concentration of which decreases sharply when the current flow is stopped. The oxygen flow-rate is estimated from the measured values of gas composition and flow-rate. The total oxygen produced can thereby be

**Figure 2.** Cell voltage variation during constant current electrolysis at 3.5 A in high silica (a) and high calcia (b) electrolyte for 4 h.

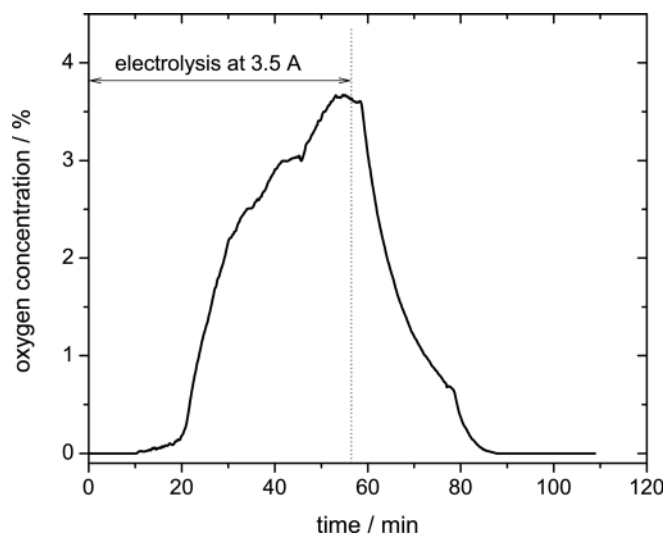


**Figure 3.** Composition of the outlet gas (average flow-rate of  $150 \text{ cm}^3/\text{min}$ ) in slag A during constant current electrolysis at 3.5 A for 1 h.

obtained and compared to the coulombic charge passed during the experiment, leading to a calculated current efficiency of  $\sim 25\%$ . The low anodic current efficiency is most likely attributable to the consumption of electrolytically produced oxygen through chemical reaction with the molybdenum crucible to form molybdenum oxide. Just the same, the data prove that oxygen is produced at a significant rate on the iridium anode, such production being directly correlated to the current flow.

**Macroscopic observations.**—The shape of the anode changes significantly after electrolysis in the high-calcia melt, whereas no noticeable changes were observed for the iridium anode used in the high-silica melt. The vertical dimension of the iridium anode in high-calcia was reduced by approximately 1 mm. The weight loss of the anode is 20 times higher in the high-calcia melt than in the high-silica, as shown in Fig. 4 (these estimations are considered to be minimum values as residual electrolyte may still be attached to the iridium anodes after electrolysis). It is also shown that this loss is not directly proportional to the electrolysis time in the high-calcia melt. The recovered cathodes from both electrolytes are coated with significant deposits, made partly of metallic and nonmetallic (oxide)

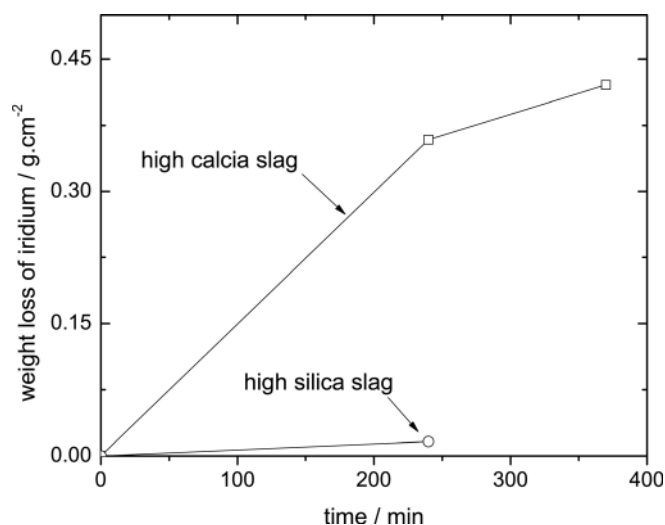


**Figure 4.** Weight loss of iridium anode, reported with reference to the total geometric surface area, in both electrolytes as a function of electrolysis time at constant current (3.5 A).

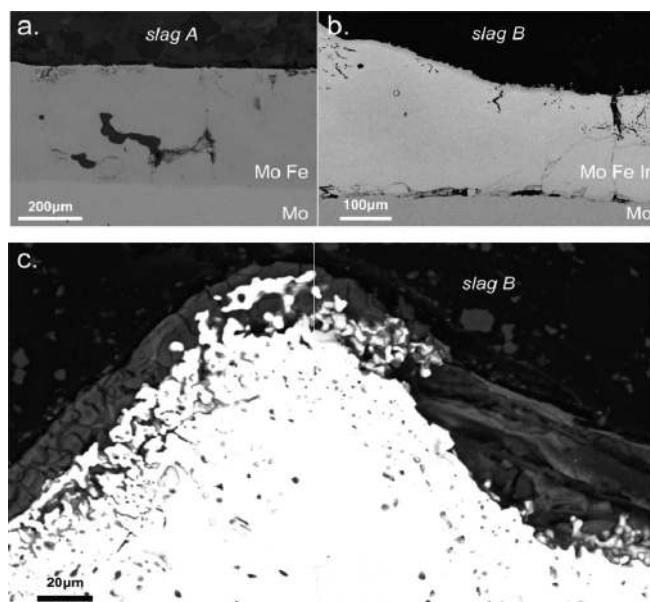


**Figure 5.** SEM observations of the cathode after electrolysis in high silica (a) and high calcia (b,c) melts.

material. A dendritic product was also observed on the cathode from electrolysis in the high-calcia electrolyte.

**Microscopic observations.**—**Cathode.** Though not the primary interest of this specific study, the cathode was subjected to characterization and analysis, as shown in Fig. 5. The deposits from both melts were similar in shape, but differed significantly in composition as determined by EDS. The deposit from the high-silica electrolyte has a composition of  $\text{Fe}_{0.48}\text{Mo}_{0.52}$  (Fig. 5a), whereas the deposit from the high-calcia electrolyte also contains iridium, the composition being  $\text{Fe}_{0.49}\text{Ir}_{0.23}\text{Mo}_{0.28}$  (Fig. 5b). In both cases, the oxygen content is lower than the detection limit of the EDS instrumentation, qualitatively proving the ability of the process to electrowin metal from molten metal oxide. The EDS analysis of the dendrites visible

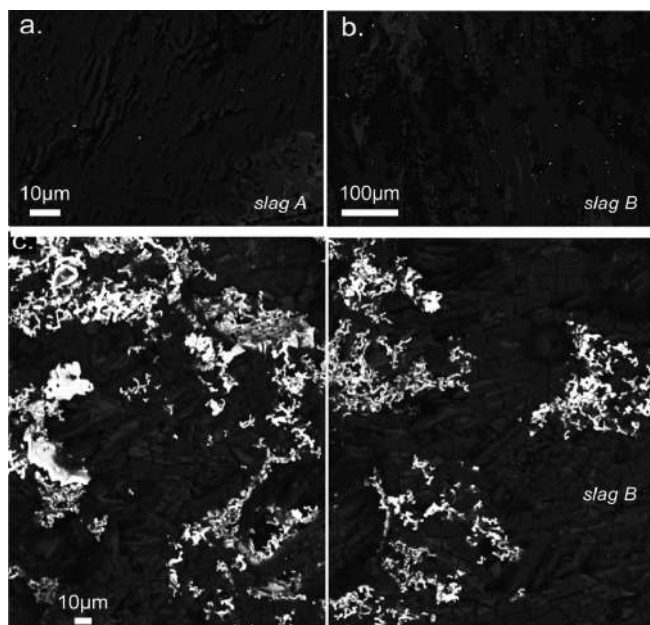


**Figure 6.** SEM observations of the electrolyte: (a) high silica, (b) high calcia slag (bulk far from anode), and (c) high calcia slag near the anode.



**Table II. Chemical analysis results (avg.  $\pm$  std., mol %) of iridium phase in each melt by SEM/EDS.**

Element	High silica melt (Slag A)		High calcia melt (Slag B)		
	Bulk anode	Near anode	Bulk anode	Near anode	Bulk electrolyte
O	1.0 ( $\pm$ 0.5)	2.4 ( $\pm$ 0.3)	5.2 ( $\pm$ 1.9)	10.4 ( $\pm$ 4.5)	16.4 ( $\pm$ 7.6)
Mg	0.5 ( $\pm$ 0.1)	0.5 ( $\pm$ 0.2)	0.3 ( $\pm$ 1.9)	1.3 ( $\pm$ 0.9)	2.2 ( $\pm$ 0.7)
Al	1.9 ( $\pm$ 0.2)	1.7 ( $\pm$ 0.1)	1.5 ( $\pm$ 0.5)	1.5 ( $\pm$ 0.6)	4.5 ( $\pm$ 1.1)
Si	1.9 ( $\pm$ 0.7)	1.6 ( $\pm$ 0.3)	2.1 ( $\pm$ 0.4)	3.6 ( $\pm$ 1.1)	3.6 ( $\pm$ 1.7)
Ca	1.0 ( $\pm$ 0.4)	1.0 ( $\pm$ 0.0)	1.6 ( $\pm$ 0.6)	1.7 ( $\pm$ 1.2)	4.6 ( $\pm$ 1.1)
Fe	1.5 ( $\pm$ 0.3)	5.0 ( $\pm$ 3.9)	1.6 ( $\pm$ 0.7)	18.9 ( $\pm$ 3.0)	15.4 ( $\pm$ 2.6)
Ir	92.1 ( $\pm$ 1.0)	87.8 ( $\pm$ 3.9)	87.7 ( $\pm$ 2.0)	62.7 ( $\pm$ 4.5)	53.2 ( $\pm$ 7.3)

to the naked eye in Fig. 5c confirms that electrolysis in a high-calcia melt will result in the transfer of iridium from the anode to the cathode. We attribute the presence of molybdenum in the metal deposit to alloying of the substrate by the liquid iron produced by electrolysis. In contrast, the presence of iridium in the metal deposit is an important indication of the instability of the anode in the high-calcia electrolyte: the possibility of an electrorefining-type process cannot be dismissed. By estimating the amount of iridium found in the cathodic product, and assuming the following overall reaction:



we calculate that the putative electrorefining of iridium consumed only  $\sim$ 3% of the total current passed during electrolysis. Therefore, such a mechanism could be operative with little effect on cathodic current efficiency.

**Electrolyte.** Characterization and analysis of the bulk electrolyte reveal the presence of particles of metallic iridium in both systems (Figs. 6a and 6b). In the high-silica melt the iridium particle size is too small ( $<1 \mu\text{m}$ ) to permit EDS to perform quantitative chemical analysis to an acceptable degree of reproducibility. In the high-calcia melt, the picture is clearer, with the iridium concentration of particles increasing closer to the anode (Fig. 6c) where they exhibit a powder-like structure. The detailed analysis of these particles is presented in Table II. There is significant contamination of the dispersed iridium metal phase with iron and oxygen. Though the oxy-

gen signal is quantitatively underestimated, the presence of an iron oxide phase hints of the mechanism responsible for the presence of iridium metal in the bulk electrolyte. Indeed, any iridium oxide phase, written here  $\text{IrO}_2$ , or cation electrochemically produced at the anode could spontaneously react with an iron suboxide to convert back to iridium metal while oxidizing iron to Fe(III). The following reaction is an example of this mechanism:



for which  $\Delta G = -271.778 \text{ kJ mol}^{-1}$  at  $1600^\circ\text{C}$ .<sup>16</sup> This spontaneous thermochemical conversion, thermodynamically favored with respect to the decomposition of iridium oxide into elemental iridium and oxygen gas for which  $\Delta G = -83.336 \text{ kJ mol}^{-1}$  at  $1600^\circ\text{C}$ ,<sup>16</sup> can also occur if gaseous iridium oxide is introduced into the electrolyte. This is a possibility given the reactivity of iridium with dry oxygen at temperatures exceeding  $1300^\circ\text{C}$ .<sup>15</sup>

**Anode.** The difference in iridium consumption between the two electrolytes can be seen Figs. 7a and 7b, where consumption on both sides at a significant level (around  $200 \mu\text{m}$ ) is evident on the anode operated in the high-calcia electrolyte. This metal loss leads to a wave-shaped surface, such morphology being potentially related to oxygen gas generation. Fractures are evident in the bulk of the iridium, but these were present in the starting material and are not the result of operation at high temperature. At higher magnifications (Figs. 7c–7d), in both electrolytes there is evidence of metal dispersion in the form of small clusters with a shape very similar to that of the metal particles observed in the bulk electrolyte (see Fig. 6c). As shown in Figs. 8a and 8b, the tip of the iridium anode operated in high-calcia electrolyte shows the most severe degradation at the thinnest cross-section near the tip. The formation of a droplet composed of finely divided metal mixed with the oxide possibly indicates the production of a gas phase on the tip where current density is expected to have been at its highest value.

Table II gives a summary of EDS analysis of iridium from the body of the anode, the particles detached from the anode (larger than  $3 \mu\text{m}$ ), and the droplets present on the tip of the anode in high-calcia electrolyte (Fig. 8). In both electrolytes, the bulk analysis reveals the presence of iridium metal with greater than background level of other oxides, iron being in a similar concentration range as the other metal cations. Interestingly, the iridium particles detached from the anode in the high-calcia melt are enriched in iron and oxygen. Their composition is similar to that of the particles found in the

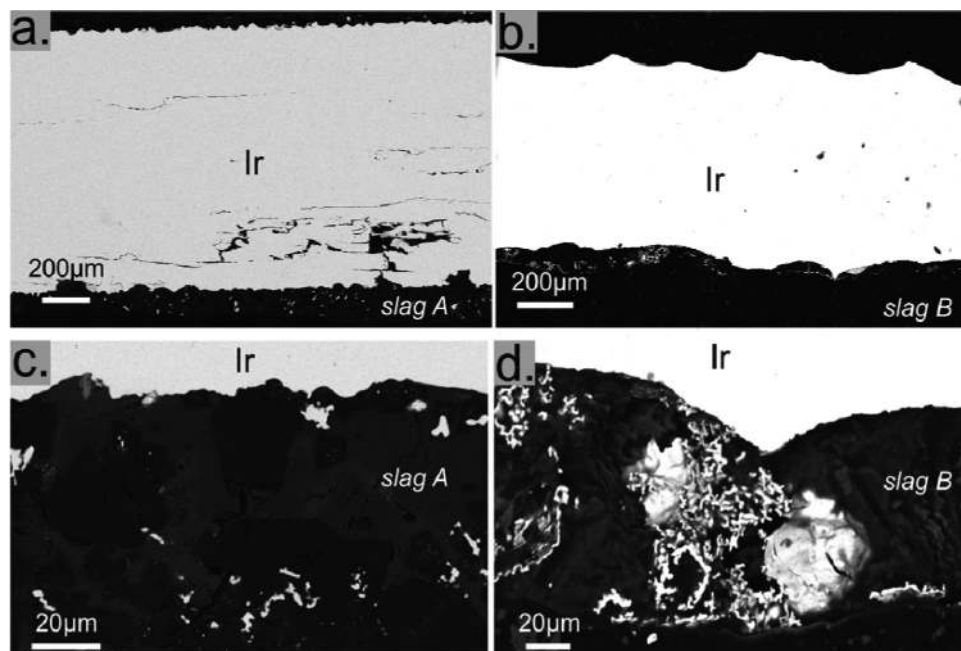


**Figure 7.** SEM observations of iridium anode after electrolysis in high silica (a,c) and high calcia (b,d).

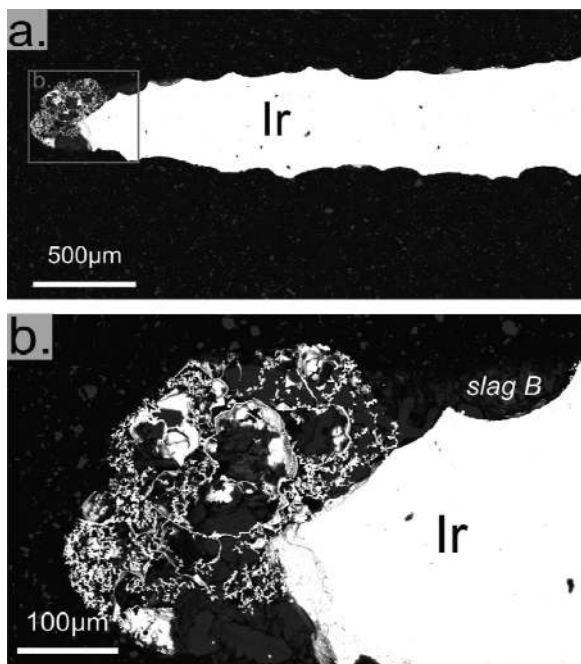
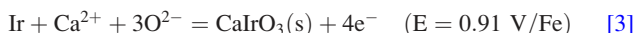


**Figure 8.** SEM observations of iridium anode tip facing the cathode, after electrolysis in high calcia melt.

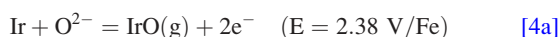
bulk electrolyte, confirming the identical nature of this material and likely the same mechanism for their generation.

### Discussion

The rate of anode consumption was shown to be dramatically different in the two electrolytes under similar experimental conditions. In slag B rich in calcia the iridium consumption rate was ~20 times greater than that in slag A rich in silica, as indicated by macroscopic weight loss measurement in Fig. 4 and microscopic analysis of the electrochemical cell components in Figs. 5–8. The two slags in this study have very different physico-chemical properties as shown in Table I. Noteworthy is the fact that slag B rich in calcia has a higher electrical conductivity and much lower viscosity than slag A rich in silica. The viscosity of the melt, for example, will influence mass transport, including the rate of delivery of oxygen-bearing ions to the electrode and the rate of removal of oxygen gas as shown in Fig. 2, while electrical conductivity will influence the kinetics of corrosion. The higher corrosion rate of iridium observed in the more basic electrolyte may be related to iridium speciation. It is known that in aqueous solutions iridate ions are expected to form at high pH leading to iridium dissolution.<sup>17</sup> Accordingly, in an oxide melt we expect the iridium corrosion mechanism to involve free oxide ions, which represent the most basic species. For example, calcium iridate may be formed in high-calcia electrolyte according to the reaction



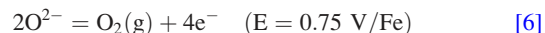
with attendant corrosion of the iridium anode.<sup>18</sup> Furthermore, at high temperature iridium metal can react with oxygen to form volatile iridium oxides as in the following reactions:



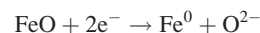
In addition, the formation of the highly stable solid iridium (IV) oxide cannot be dismissed:



Finally, oxygen evolution according to Eq. (6) is the desirable reaction for an inert-anode:



Cell voltages for the above reactions were evaluated against a common cathode reaction:



Electrode potentials at 1600°C were calculated from Gibbs free energies of the relevant stoichiometric compounds compiled in the HSC Database.<sup>16</sup>

Altogether, our findings support a fundamental role of the chemistry of the electrolyte on iridium stability. Reactions (3) and (4c) should directly be favored with respect to (6) only in highly basic electrolytes which have high concentrations of  $\text{O}^{2-}$ . This observation is in agreement with the results recently obtained for increased rhodium dissolution in high basicity slag.<sup>19</sup>

### Conclusion

Iridium is seen as a candidate material for an oxygen-evolving anode only in acidic melts. Basic melts attack iridium owing to the high concentration of free oxide ion coupled with the low viscosity, which results in unimpaired mass transport.

### Acknowledgments

The present work is part of the American Iron and Steel Institute (AISI) CO<sub>2</sub> breakthrough program.

### References

- J.-P. Birat, J. Borlée, B. Korhas, J. Stel, K. Meijer, C. Günther, M. Halin, T. Bürgler, H. Lavelaine, C. Treadgold, I. Millar, D. Sert, T. Torp, F. Patisson, B. Paya, and E. Burstrom, in *3rd International Conference on Process Development in Iron and Steelmaking*, Luleå, Sweden (2008).
- A. Allanore, H. Lavelaine, G. Valentin, J. P. Birat, and F. Lapique, *J. Electrochem. Soc.*, **155**(9) (2008).
- G. M. Haarberg, E. Kvalheim, S. Rolseth, T. Murakami, S. Pietrzyk, and S. Wang, *ECS Trans.*, **3**(35), 341 (2007).
- D. Wang, A. J. Gmitter, and D. R. Sadoway, *J. Electrochem. Soc.*, **158**, E51 (2011).
- D. R. Sadoway, *J. Mater. Res.*, **10**, 487 (1995).
- J. Di Martino, C. Rapin, P. Berthod, R. Podor, and P. Steinmetz, *Corros. Sci.*, **46**, 1849 (2004).
- J. Di Martino, C. Rapin, P. Berthod, R. Podor, and P. Steinmetz, *Corros. Sci.*, **46**, 1865 (2004).
- A. J. Gmitter, in *Material Science and Engineering*, MIT, Cambridge (2008).
- S. L. Schiefelbein, N.A. Fried, K.G. Rhoads, and D.R. Sadoway, *Rev. Sci. Instrum.*, **69**, 3308 (1998).
- S. L. Schiefelbein, N. A. Fried, K. G. Rhoads, and D. R. Sadoway, *Metall. Mater. Trans. B*, **28**, 1141 (1997).
- Slag Atlas*, V. D. Eisenhüttenleute, Editor., 2nd ed., Verlag Stahleisen (1995).
- J. A. Duffy, *Geochim. Cosmochim. Acta*, **57**, 3961 (1993).
- Y. Waseda and J. M. Toguri, *The Structure and Properties of Oxide Melts: Application of Basic Science to Metallurgical Processing*, World Scientific, Singapore, River Edge, NJ (1998).
- C. W. Bale and A. D. Pelton, FactSage 6.1 (2009).
- M. S. Chandrasekharaiah, M. D. Karkhanavala, and S. N. Tripathi, *J. Less-Common Met.*, **80**, P9 (1981).
- A. Roine, HSC chemistry, 6.00, Outokumpu (2007).
- M. Pourbaix, Atlas of Electrochemical Equilibria in Aqueous Solutions. 1974, Houston: National Association of Corrosion Engineers.
- K. T. Jacob et al., *J. Electrochem. Soc.*, **146**(5), 1854 (1999).
- C. Wiraseranee, T. H. Okabe, K. Morita, *2nd International Symposium on High-Temperature Metallurgical Processing*, TMS, Warrendale, PA, pp. 143–150 (2011).